SEDIMENTOLOGY the journal of the International Association of Sedimentologists

Sedimentology (2017) **64**, 168–185 doi: 10.1111/sed.12352

Patterns of local and global redox variability during the Cenomanian–Turonian Boundary Event (Oceanic Anoxic Event 2) recorded in carbonates and shales from central Italy

JEREMY D. OWENS*, TIMOTHY W. LYONS†, DALTON S. HARDISTY†[1], CHRIS M. LOWERY‡, ZUNLI LU§, BRIDGET LEE† and HUGH C. JENKYNS¶
**Department of Earth, Ocean and Atmospheric Science & National High Magnet Field Laboratory, Florida State University, Tallahassee, FL 32306, USA (E-mail: jdowens@fsu.edu)*
†Department of Earth Sciences, University of California, Riverside, Riverside, CA 9221, USA
‡Institute for Geophysics, The University of Texas at Austin, Austin, TX 7878, USA
§Earth Science Department, Syracuse University, Syracuse, NY 13244, USA
¶Department of Earth Sciences, University of Oxford, Oxford OX1 3AN, UK

Associate Editor – Ulrich Heimhofer

ABSTRACT

Careful evaluation of the local geochemical conditions in past marine settings can provide a window to the average redox state of the global ocean during episodes of extensive organic carbon deposition. These comparisons aid in identifying the interplay between climate and biotic feedbacks contributing to and resulting from these events. Well-documented examples are known from the Mesozoic Era, which is characterized by episodes of widespread organic carbon deposition known as Oceanic Anoxic Events. This organic carbon burial typically leads to coeval positive carbon-isotope excursions. Geochemical data are presented here for several palaeoredox proxies (Cr/Ti, V, Mo, Zn, Mn, Fe speciation, I/Ca and sulphur isotopes) from a section exposed at Furlo in the Marche–Umbrian Apennines of Italy that spans the Cenomanian–Turonian boundary. Here, Oceanic Anoxic Event 2 is represented by a *ca* 1 m thick radiolarian-rich millimetre-laminated organic-rich shale known locally as the Bonarelli Level. Iron speciation data for thin organic-rich intervals observed below the Bonarelli Level imply a local redox shift going into the Oceanic Anoxic Event, with ferruginous conditions (i.e. anoxic with dissolved ferrous iron) transiently developed prior to the event and euxinia (i.e. anoxic and sulphidic bottom waters) throughout the event itself. Pre-Oceanic Anoxic Event enrichments of elements sensitive to anoxic water columns were due to initial development of locally ferruginous bottom waters as a precursor to the event. However, the greater global expanse of dysoxic to euxinic conditions during the Oceanic Anoxic Event greatly reduced redox-sensitive trace-metal concentrations in seawater. Pyrite sulphur isotopes document a positive excursion during the Oceanic Anoxic Event. Carbonate I/Ca ratios were generally low, suggesting locally reduced bottom-water oxygen conditions preceding the event and relatively increased oxygen concentrations post-event. Combined, the Furlo geochemical data suggest a redox-stratified water column with oxic surface waters and a shallow chemocline overlying locally ferruginous bottom waters preceding the event, globally widespread euxinic bottom waters during the Oceanic

[1]Present address: Woods Hole Oceanographic Institution, Woods Hole, Massachusetts 02543, USA

Anoxic Event, followed by chemocline shallowing but sustained local redox stratification following the event.

Keywords Geochemistry, Oceanic Anoxic Event, Oceanic Anoxic Event 2, redox conditions, sulphur, trace metals.

INTRODUCTION

Sediments linked to the Cenomanian–Turonian boundary are well exposed at Furlo Gorge in Marche–Umbria, central Italy (Fig. 1), with a nearly 30 m thick succession containing foraminiferal–nannofossil limestone, chert and organic-rich facies, including a *ca* 1 m thick black shale/radiolarian sand unit (Bonarelli Level) representing the local expression of Oceanic Anoxic Event 2 (OAE 2; Beaudoin *et al.*, 1996; Turgeon & Brumsack, 2006; Lanci *et al.*, 2010; Gambacorta *et al.*, 2015). Oceanic Anoxic Event 2 represents the most severe global climatic perturbation in the Cretaceous Period (Schlanger *et al.*, 1987; Kuroda & Ohkouchi, 2006; Takashima *et al.*, 2006; Jenkyns, 2010), marked by globally distributed organic carbon deposition (Schlanger & Jenkyns, 1976) that is expressed in a large coeval positive carbon-isotope excursion in marine carbonates and marine and terrestrial organic matter (Scholle & Arthur, 1980; Arthur *et al.*, 1990; Hasegawa, 1997). The event is generally marked by indicators of relatively elevated temperatures and atmospheric CO_2 (Berner, 2006; Takashima *et al.*, 2006; Friedrich *et al.*, 2012), high sea level (Haq *et al.*, 1987; Jarvis *et al.*, 2001), enhanced phosphorus regeneration/recycling (Van Cappellen & Ingall, 1994; Nederbragt & Fiorentino, 1999; Mort *et al.*, 2008; Kraal *et al.*, 2010), increased hydrothermal activity or other forms of basalt–seawater interaction (Jones & Jenkyns, 2001; Snow *et al.*, 2005; Kuroda *et al.*, 2007; MacLeod *et al.*, 2008; Du Vivier *et al.*, 2014, 2015; Jenkyns *et al.*, 2017), increased continental weathering (Blättler *et al.*, 2011; Blumenberg & Wiese, 2012; Pogge von Strandmann *et al.*, 2013) and major changes in the movement of marine water masses (Martin *et al.*, 2012;

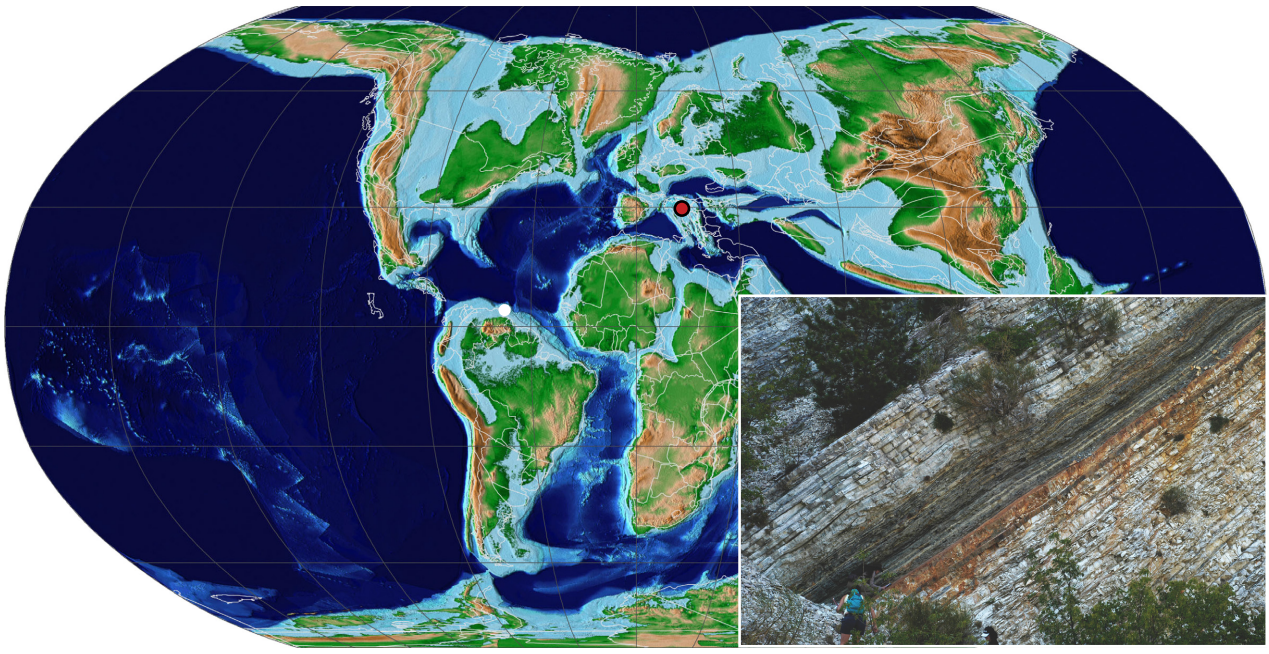

Fig. 1. Palaeogeographic locations of Furlo (red circle) and Demerara Rise (white circle) adapted from the PALEOMAP Project (Scotese, 2008) with an inset photograph of the Furlo outcrop, illustrating the Bonarelli Level (*ca* 1 m thick) and the underlying and overlying grey pelagic limestones (the so-called Scaglia) at the time of sampling.

Zheng *et al.*, 2013). The physical and chemical oceanographic changes during the OAE resulted in evolutionary turnover of marine organisms, including molluscs (Elder & Kirkland, 1985; Elder, 1991), calcareous nannofossils (e.g. Bralower, 1988; Erba, 2004), radiolarians (Erbacher *et al.*, 1996; Erbacher & Thurow, 1997; Musavu-Moussavou *et al.*, 2007) and benthonic and planktonic foraminifera (e.g. Leckie, 1985; Kaiho & Hasegawa, 1994; Premoli Silva & Sliter, 1999; Leckie *et al.*, 2002; Parente *et al.*, 2008).

Understanding the dynamics of de-oxygenation during this short-lived event, estimated as lasting between 450 kyr and 900 kyr (Arthur & Premoli-Silva, 1982; Kuhnt *et al.*, 2005; Sageman *et al.*, 2006; Voigt *et al.*, 2008; Eldrett *et al.*, 2015; Batenburg *et al.*, 2016), and similar organic carbon burial events throughout Earth history, has been a major priority in the search to unravel the climate forcing, biological feedbacks and related redox dynamics of the ocean during biotic extinction events (Bambach, 2006). There is mounting evidence for widespread anoxic and specifically euxinic conditions during OAE 2 based on diverse geochemical proxies for local bottom-water redox at multiple locations (Brumsack, 2006; Turgeon & Brumsack, 2006; Jenkyns *et al.*, 2007; van Bentum *et al.*, 2009; Pearce *et al.*, 2009; Lu *et al.*, 2010; Hetzel *et al.*, 2011; Owens *et al.*, 2012, 2016; Westermann *et al.*, 2014; Dickson *et al.*, 2016a; Goldberg *et al.*, 2016), including evidence for photic-zone euxinia (Sinninghe Damsté & Köster, 1998; Kuypers *et al.*, 2002; Pancost *et al.*, 2004; van Bentum *et al.*, 2009). Numerical ocean modelling suggests that 50% (by volume) of the global ocean was anoxic during the OAE (Monteiro *et al.*, 2012). However, sulphur-isotope and molybdenum-isotope mass balance models suggest more limited extents of euxinia, specifically with a maximum of 7% of the sea floor (Owens *et al.*, 2013; Dickson *et al.*, 2016a,b). By contrast, the global redox conditions prior to and following the OAE remain less known, although several studies have suggested reduced oceanic oxygenation prior to the event (Lu *et al.*, 2010; Westermann *et al.*, 2014; Zhou *et al.*, 2015; Owens *et al.*, 2016). This possibility is particularly relevant as the observed turnover of radiolaria began well before the event, biotic turnover of microfossil groups just before the onset of the OAE (Coccioni *et al.*, 2016) and the main biotic turnover recorded in the middle of the Bonarelli Level (Erbacher & Thurow, 1997; Musavu-Moussavou *et al.*, 2007). The decline of other fossil groups during the OAE has been attributed to an expansion of anoxic and euxinic conditions that were unfavourable and even toxic to life (Leckie *et al.*, 2002; Snow *et al.*, 2005). Furthermore, the wide extent of euxinia during the OAE appears to have drawn down bio-essential trace metals (Algeo & Maynard, 2004; Reinhard *et al.*, 2013; Owens *et al.*, 2016), which are important for nitrogen fixation (Fe, Mo and V; Zerkle *et al.*, 2006; Bellenger *et al.*, 2011) and play an integral role in controlling primary production.

The data set presented here combines several geochemical tracers of marine redox from both shales and carbonates with the goal of constraining local surface-water and bottom-water redox conditions prior to, during and subsequent to the OAE, as well as the global redox landscape during this event. Historically, it has been difficult to assess the stratigraphic record of oxygen dynamics leading into and out of the OAEs due to lithological changes – specifically, transitions from carbonates to organic-rich shales and back to carbonates. Many of the most widely used palaeoredox proxies were developed for use with shales. Recently, however, there have been significant geochemical advances towards more robust assessments of local and global oxygen conditions recorded in carbonate lithologies (Lu *et al.*, 2010; Gill *et al.*, 2011a,b; Owens *et al.*, 2013; Hardisty *et al.*, 2014; Zhou *et al.*, 2015).

The $\delta^{13}C_{organic}$ proxy is used specifically in this study as a tracer for global burial of isotopically light organic carbon and as a reliable tool for stratigraphic correlation. Furthermore, shale iron geochemistry is used to inform local redox conditions that allows for a more sophisticated interpretation of trace-metal geochemistry. In particular, armed with independent constraints on local redox conditions, interpretations of trace-metal enrichments allow tracking of global redox shifts between oxic, anoxic (V, Cr/Ti, Zn) and euxinic (Mo) conditions. Lastly, integration of carbonate-associated sulphur (CAS) isotopes, a proxy for the global biogeochemical sulphur cycle, and carbonate I/Ca proxy as a fingerprint of local oxic versus anoxic conditions and the relative chemocline position, provide additional constraints. Finally, pyrite $\delta^{34}S$ has the potential to constrain local environmental conditions, and $\Delta^{34}S$, the isotopic difference between marine sulphate (from CAS) and pyrite, can provide additional environmental information, such as marine sulphate concentration as related to the extent of marine anoxia and associated pyrite burial.

MATERIALS AND METHODS

Geological setting

This study focused on sedimentary rocks from the Marche–Umbria region of Italy near the village of Furlo (Fig. 1) – specifically, outcrops exposed in a disused quarry located approximately 25 km south-east of Urbino. The exposed rocks are pelagic deposits laid down on the continental margins of the Tethyan Ocean (Bernoulli & Jenkyns, 2009). Of particular interest is the Bonarelli Level, represented by a 110 cm thick laminated organic-rich interval with clay and thin radiolarian sands (Turgeon & Brumsack, 2006; Jenkyns *et al.*, 2007; Mort *et al.*, 2007; Lanci *et al.*, 2010). Carbonates and organic-rich facies were sampled extending *ca* 12·5 m below the base of the Bonarelli Level, where the section consists of: (i) rhythmic layers or couplets of alternating light grey micritic limestone rich in nannofossils and planktonic foraminifera (the so-called Scaglia Bianca); (ii) black and grey chert; and (iii) intercalated thin (millimetre to centimetre) black organic-rich shales (Beaudoin *et al.*, 1996; Jenkyns *et al.*, 2007; Mitchell *et al.*, 2008; Gambacorta *et al.*, 2015). These thin black shales constitute only a few per cent of the section by thickness and are missing in many other OAE 2 localities in Marche–Umbria; their presence elevates the value and novelty of this study. The overall sequence shows a cyclic stratigraphic pattern of cherts, shales and limestones, which is attributed to astronomical forcing in the Alpine Tethys–Central Atlantic Ocean. Specifically, the thin black shale levels have been assigned to formation during eccentricity minima with reduced deep-water circulation favouring transient anoxia (Lanci *et al.*, 2010).

The samples were collected in the middle of individual facies to avoid any gradational redox effect associated with adjacent lithologies, but generally the boundaries between lithological units are sharp and distinct. For this study, all of the chert-dominated layers were avoided, because they are not well-suited to proxy approaches used here. Five carbonate samples were collected from above the top of the Bonarelli Level. Weathered surfaces were avoided for all samples collected, especially the carbonate-lean shale intervals, in order to minimize any post-depositional oxidation effects that would most adversely affect Fe speciation. Additionally, for the Bonarelli Level itself, the samples were excavated as deeply as possible (generally 5 to 7 cm) to reveal the freshest non-fissile material, which is less likely to have been exposed to post-depositional oxidation. This approach was deemed especially important because of the likelihood of pyrite oxidation given that the rocks below the black shale are stained rust orange (Fig. 1).

Methods

Samples of both carbonates and organic-rich shales were collected for whole-rock geochemical analysis. All samples were trimmed prior to powdering to ensure that geochemical analyses were performed on the most pristine materials possible. All samples were powdered using a trace-metal-clean ball mill. For organic carbon isotopes ($\delta^{13}C_{org}$), all samples were decarbonated using 4 M hydrochloric acid until effervescence ceased. The samples were then rinsed several times using deionized water and ultimately combusted by elemental analyser (EA) coupled, under continuous flow, to a Delta V Thermo IRMS (Isotope Ratio Mass Spectrometer; Thermo Fisher Scientific, Waltham, MA, USA) at the University of California, Riverside. The isotope ratio ($^{13}C/^{12}C$) was calculated as:

$$\delta^{13}C(‰) = \left[\frac{^{13}C/^{12}C_{sample}}{^{13}C/^{12}C_{standard}} - 1\right] \bullet 1000 \qquad (1)$$

All values are presented in the standard delta notation as per mil (‰) deviation from Vienna Pee Dee Belemnite (V-PDB), with replicate analyses yielding a standard deviation of 0·05‰. Total carbon (TC) and total sulphur (TS) were measured by combustion of 100 mg of sample in an Eltra CS-500 carbon/sulphur analyser with high-temperature furnace (1400°C; Eltra GmbH, Haan, Germany). Total inorganic carbon (TIC) was measured using an acidification module in combination with the Eltra instrument, and total organic carbon (TOC) was calculated as the difference between TC and TIC.

A standard chromium reduction method was used to quantify pyrite sulphur concentrations (Canfield *et al.*, 1986). Chromium reduction was performed on all bulk samples of organic-rich shale, as well as the residue remaining following the CAS extraction (see below). Specifically, pyritic sulphur (S_{pyrite}) was extracted using a boiling solution of chromous chloride with hydrochloric acid for 2 h, a technique that evolves hydrogen

sulphide gas. This sulphide was trapped by precipitation as zinc sulphide (ZnS). The precipitate was quantified by titration, yielding wt% S_{pyrite}. For isotopic analysis of $\delta^{34}S_{pyrite}$, the hydrogen sulphide was instead precipitated as silver sulphide using the same chromium reduction method but with a solution trap containing silver nitrate with ammonium hydroxide.

All samples analysed for $\delta^{34}S_{CAS}$ contained carbonate contents greater than 65 wt% and up to 95 wt%. A standard procedure was followed for extracting CAS (Gellatly & Lyons, 2005; Gill *et al.*, 2011a,b). Briefly, *ca* 10 to 20 g of powdered sample was treated with a solution of 10% sodium chloride and then 125 ml of concentrated sodium hypochlorite, and each step was followed by multiple rinses of deionized water to prevent the incorporation of any non-CAS sulphur-bearing phases. The samples were then dissolved using 4 M hydrochloric acid for less than 1 h and immediately vacuum-filtered, minimizing any oxidation of pyrite. Pyrite oxidation was further limited by the low ferric iron contents of the samples and generally low amounts of pyrite. A barium chloride solution was added to precipitate the extracted sulphate as barium sulphate.

The precipitated silver sulphide and barium sulphate was filtered, homogenized and weighed into pressed tin capsules with excess vanadium pentoxide. The samples were combusted by EA coupled, under continuous flow, to a Delta V Thermo IRMS. The isotope ratio ($^{34}S/^{32}S$) was calculated as:

$$\delta^{34}S(‰) = \left[\frac{^{34}S/^{32}S_{sample}}{^{34}S/^{32}S_{standard}} - 1\right] \bullet 1000 \qquad (2)$$

All sulphur-isotope compositions are reported in standard delta notation as per mil (‰) deviation from Vienna Canyon Diablo Troilite (V-CDT). The data were analysed in the Lyons stable isotope laboratory at the University of California, Riverside, using a series of in-house standards (IAEA S-1, S-2 and S-3) and international standards (IAEA SO-5, IAEA SO-6 and NBS 127), with a replicate analyses agreement of 0·2‰ or better.

Trace-element analysis was performed using *ca* 100 mg of powder weighed into ceramic vials and heated for *ca* 12 h at 450°C to volatilize all organic material. The samples were subsequently weighed after cooling to determine the loss on ignition and then transferred into trace-metal-clean Savillex vials (Savillex Corporation, Eden Prairie, MN, USA) and completely dissolved using a standard sequential acid protocol (nitric acid/hydrochloric acid/hydrofluoric acid) at *ca* 150°C. Subsequent to complete dissolution, the samples were dried down and then reconstituted in *ca* 0·35 M HNO_3 for major-element and trace-element analysis. All acids used in this method were Aristar/trace-metal grade. Elemental concentrations (Al, Fe, Ti, Mo, V, Cr and Zn) were measured using an Agilent 7500ce quadrupole inductively coupled plasma mass spectrometer (ICP-MS; Agilent Technologies, Santa Clara, CA, USA) housed in the Lyons' laboratory at the University of California, Riverside. Standard reference materials (SDO-1 shale) were digested along with the samples and analysed with each batch of digestions, and were within the accepted analytical error for all elements. Procedural blanks were below detection limits, and analytical reproducibility on separate dissolved samples was better than 5% for all elements.

Iron speciation analysis was performed on all of the shale samples. According to convention, this study operationally defines highly reactive iron (Fe_{HR}) as pyrite Fe (Fe_{py}), Fe carbonate (Fe_{carb}), Fe oxides (Fe_{ox}) and magnetite Fe (Fe_{mag}). All of these phases are assumed to be reactive towards hydrogen sulphide on early diagenetic timescales (Canfield *et al.*, 1992; Raiswell & Canfield, 1998; Poulton & Canfield, 2005). Highly reactive iron is thus calculated as $Fe_{py} + Fe_{carb} + Fe_{ox} + Fe_{mag}$. Pyrite Fe concentrations are calculated using the chromium method described above, with Fe_{py} calculated from the pyrite S concentrations assuming a stoichiometry of FeS_2. Unpyritized reactive Fe (Fe_{carb}, Fe_{ox} and Fe_{mag}) was analysed using a three-step sequential extraction (Poulton & Canfield, 2005; Poulton & Raiswell, 2005). Briefly, *ca* 100 mg of sample was weighed into a 15 ml centrifuge tube and processed as follows: (i) a 1 M sodium acetate extraction adjusted to a pH of 4·5 with constant shaking for 24 h to extract Fe_{carb}; (ii) extraction of the sample residue for Fe_{ox} using 50 g l^{-1} sodium dithionite buffered to a pH of 4·8 for 2 h with constant shaking; and (iii) extraction of Fe_{mag} from the remaining residue using an ammonium oxalate/oxalic acid-buffered solution at a pH of 3·2 for 6 h. All extracts were analysed using an ICP-MS in the Lyons laboratory.

Iodine/calcium ratios (I/Ca) in carbonate lithologies were determined by quadrupole ICP-

MS (Bruker M90; Bruker Corporation, Billerica, MA, USA) at Syracuse University. Measurements of iodine and calcium were determined by dissolving *ca* 1 to 5 mg of sample in trace-metal-clean vials using 0·54 M nitric acid (Lu *et al.*, 2010). Tertiary amine (0·5%) was added to all samples and standards to stabilize iodine, because it is volatilized in acidic solutions. The resulting solutions were analysed the same day. Standard reference materials (JCP-1 coral) were digested along with the samples and analysed in parallel, which resulted in an average iodine value of 5·59 ± 0·11 ppm (n = 5), which is similar to previous results of 5·47 ± 0·07 ppm (Lu *et al.*, 2010) and 5·5 ± 0·2 ppm (Chai & Muramatsu, 2007). The sample reproducibility was better than 5% for both I and Ca.

RESULTS

Carbon

The $\delta^{13}C_{org}$ analyses at Furlo reveal a *ca* 4‰ excursion across the organic-rich Bonarelli Level that marks the OAE at this locality. Below this organic-rich unit, within the thin black shales interbedded between the pelagic limestones, the values range between −28·1‰ and −26·4‰, with an average of −27·4‰. Within the Bonarelli Level, values range between −26·5‰ and −23·4‰, with an average of −24·8‰ (Fig. 2). These values agree well with data in Jenkyns *et al.* (2007) from the same location. The TOC values below and above the Bonarelli Level (black shales and carbonates below; carbonate above) are all below 2·2 wt%, and a majority of the samples are near 0·5 wt%. In contrast, the TOC values increase to an average of 7·0 wt% in the Bonarelli Level itself, with a maximum recorded value of 13·4 wt%. The carbonate content of the sub-Bonarelli Level black shales were all below 33 wt%, and the carbonates below and above the Bonarelli Level had averages of 90·7 wt% and 78·7 wt%, respectively. Carbonate contents for the Bonarelli Level itself were below the detection limit and are reported as zero. Jenkyns *et al.* (2007) reported TOC values between 0 and 20 wt% in the stratigraphically lower thin black shales, implying considerable non-homogeneity in these organic-rich levels. Elsewhere in Marche–Umbria, TOC contents of parts of the Bonarelli Level locally exceed 20 wt% (Farrimond *et al.*, 1990; Tsikos *et al.*, 2004; Gambacorta *et al.*, 2015).

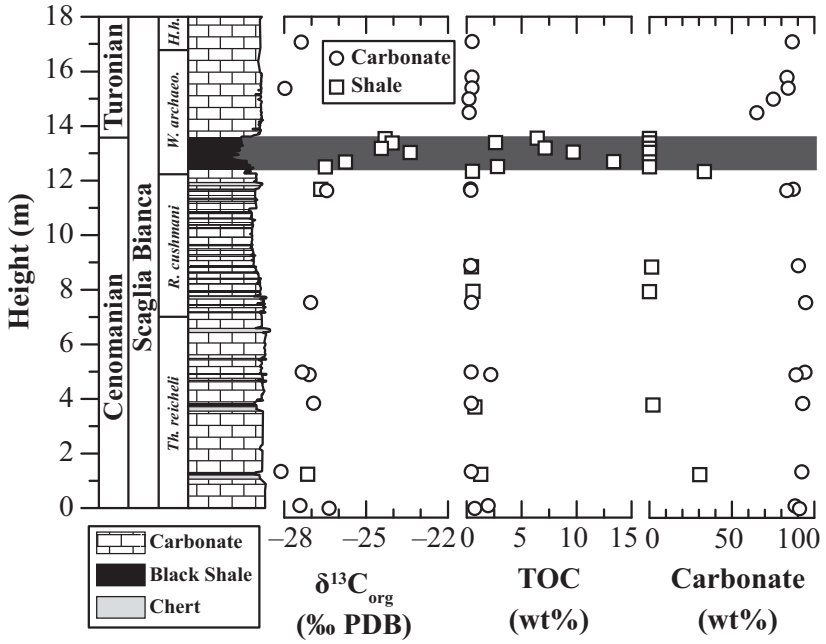

Fig. 2. Organic carbon isotopes ($\delta^{13}C_{org}$) from both shales (squares) and carbonates (circles). Total organic carbon and carbonate data for both the organic-rich shales and carbonates. Total organic carbon is low before the OAE (denoted with the dark grey bar) in both lithologies and increases during the OAE (shales). The stratigraphic column was based on the field campaign for this study but is similar to previous studies (Jenkyns *et al.*, 2007; Mort *et al.*, 2007).

Iron and trace-metal geochemistry

Iron and trace-metal analyses were performed on all samples with carbonate contents below 35 wt%, which included all organic-rich shales. These samples all had total Fe (Fe_T) contents in excess of 0·5 wt%, which is consistent with established protocols (Clarkson *et al.*, 2014). Normalizing Fe_T to Al can reveal enrichments beyond the detrital average, which for Phanerozoic mudstones and shales is 0·51 (±0·1; Raiswell *et al.*, 2008), and thereby suggesting anoxic deposition (Lyons & Severmann, 2006). Shales deposited before the OAE have an average ratio of 0·49, with a range from 0·44 to 0·51 within the Bonarelli Level itself; however, the shales have an average of 0·85 and range from 0·52 to 1·18.

The ratio of highly reactive Fe (Fe_{HR}) to Fe_T can also indicate anoxic depositional conditions because of the comparatively large proportion of reactive Fe that is typical of such settings (Raiswell & Canfield, 1998; Poulton & Canfield, 2011). Modern marine muds deposited under oxic conditions have an upper limit of 0·38 for Fe_{HR}/Fe_T (Raiswell & Canfield, 1998). The black shales below the Bonarelli Level average 0·57, with all samples above 0·50, and during the event average 0·68, with a range of 0·55 and 0·82. For all but one sample, 90% of the Fe_{HR} is from the pools of Fe_{py}, Fe_{carb} and Fe_{ox} so that Fe_{mag} makes up a small portion of the reactive Fe pool. Furthermore, the removal of Fe_{mag} from the calculations has minimal effects on the ratios and interpretations. It is unlikely that these values are driven by diagenetic artefacts because there is a large amount of pyrite and minimal amounts of secondary oxides as the magnetite contents are low. The ratio of pyrite Fe (Fe_{py}) to Fe_{HR} is a measure of the fraction of the reactive Fe pool that has been pyritized through exposure to hydrogen sulphide. Values above 0·7, when combined with elevated ratios of Fe_{HR}/Fe_T, convincingly point to deposition beneath euxinic waters (März *et al.*, 2008; Poulton & Canfield, 2011). Black shales deposited prior to deposition of the Bonarelli Level have Fe_{py}/Fe_{HR} ratios averaging 0·48, with a range between 0·40 and 0·53, whereas those recording the OAE average 0·78, with all values above 0·73 (Fig. 3). The average pyrite S concentrations in the black shales below the Bonarelli Level are 0·17 wt%, whereas in the OAE interval the average is 0·79 wt%, with a maximum value of 1·01 wt%. These high pyrite contents also attest to the freshness of the samples, consistent with the lack of obvious signs of post-depositional oxidation for the Bonarelli Level black shales.

Trace-metal analysis of the organic-rich shales at Furlo also informs investigation of the depositional redox conditions (Fig. 3). Manganese concentrations in sediments deposited prior to the OAE (average of 190 ppm) are well below the average shale value of 850 ppm (Turekian & Wedepohl, 1961) and drop to 32 ppm within the Bonarelli Level itself. Vanadium is enriched in pre-OAE black shales (578 ppm) compared to average shale values of 130 ppm (Turekian &

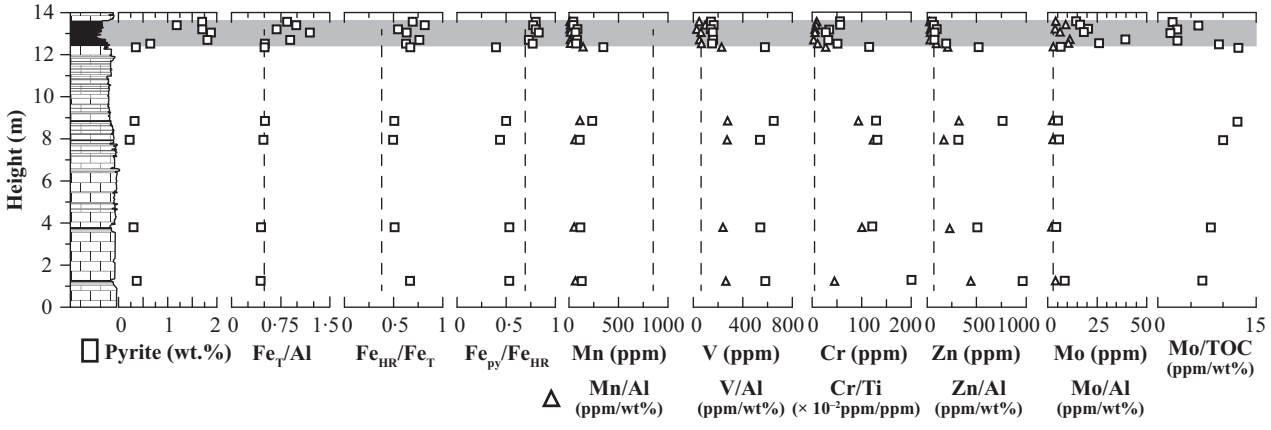

Fig. 3. Palaeoredox geochemical data from the organic-rich black shales. The Bonarelli Level recording the OAE is denoted by the grey bar and nearly all of the parameters show a major perturbation, with the Fe proxies increasing and Mo illustrating a small increase in concentration. The low-oxygen trace-metal proxies, Mn, V, Cr/Ti and Zn, all show a significant decline in concentration during the event, attributed to global drawdown of these elements due to worldwide increase of euxinic sinks. The dashed vertical lines represent the average shale value for elemental concentration except for Cr, which is based on Cr/Ti values. Triangles represent trace-metal concentrations normalized to either aluminum or titanium.

Wedepohl, 1961). Similarly, average Cr/Ti is also enriched prior to the OAE black shales (77×10^{-2} ppm/ppm) compared to the normalized average shale of Cr/Ti of $2{\cdot}0 \times 10^{-2}$ (ppm/ppm) (Turekian & Wedepohl, 1961). Chromium is normalized to Ti content due to substantial detrital inputs (Reinhard *et al.*, 2013). Averages for V and Cr/Ti in the Bonarelli Level are 152 ppm and 7×10^{-2} (ppm/ppm), respectively. Prior to the OAE, Zn concentrations range from 314 to 964 ppm (compared to 95 ppm for average shale; Turekian & Wedepohl, 1961), with an average of 613 ppm. Zinc averages 91 ppm in the Bonarelli Level, with a range of 48 to 191 ppm. Black shales deposited prior to the OAE have an average Mo content of 6 ppm with the highest value reaching 9 ppm (compared to 2·6 ppm for average shales; Turekian & Wedepohl, 1961) and Mo content averages 22 ppm with a range from 14 to 40 ppm within the Bonarelli Level. Aluminium concentrations average 1·15 wt% in the black shales prior to the OAE and show a slight increase within the Bonarelli Level (average of 1·61 wt%). These Al concentrations are low compared to the average upper continental crustal composition (8·00 wt%; Turekian & Wedepohl, 1961), a phenomenon that has been documented previously at this and nearby locations (Turgeon & Brumsack, 2006; Westermann *et al.*, 2014). This observation is probably due to dilution from organic matter and siliceous radiolarians. The ratios of a given metal to Al do not significantly alter the trends (Fig. 3) or the interpretations if compared with the absolute concentrations, although normalization does smooth some of the overall trends.

The averages and ranges herein for trace-metal contents in the pre-OAE organic-rich layers and the Bonarelli Level are similar to those reported previously from this location (Turgeon & Brumsack, 2006) and a nearby section (Westermann *et al.*, 2014), with Zn being the lone exception. Average Zn data for the Bonarelli Level are lower compared with earlier reports even though they are from the same site and similar lithologies (Turgeon & Brumsack, 2006), but the average values of the thin black shales prior to the OAE are similar. Directly comparing and using trace-metal enrichments to resolve local redox environments is challenging because the local conditions, i.e. Fe speciation, may not be completely resolved at all sites due to possible global trace-metal drawdown during the event (see *Discussion*).

Pyrite sulphur isotopes

Pyrite isotope data were generated from all of the black shales (Fig. 4). Also, a few of the carbonate samples yielded enough pyrite to determine an isotopic value, but the concentrations

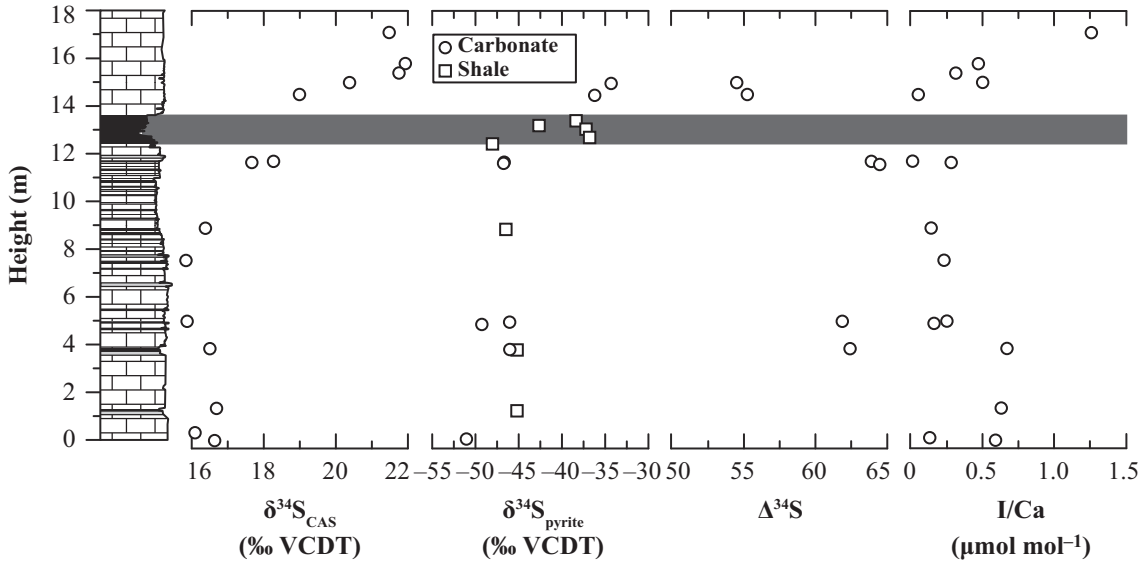

Fig. 4. Sulphur-isotope and carbonate geochemical palaeoredox data. The sulphur-isotope data shift to more positive values leading into the Bonarelli Level and increase post-OAE level, albeit with a decline in $\Delta^{34}S$. The ratio of I/Ca shows significant scatter but generally the interval below the Bonarelli Level shows relatively low values, indicating deposition in an oxygen-depleted environment for the pelagic limestones, before rebounding to higher values at the top of the section.

were too low to measure the amount of pyrite using the gravimetric method. Generally, the average $\delta^{34}S_{pyrite}$ values for carbonate and shale are in good agreement, but carbonates show greater variability. Average $\delta^{34}S_{pyrite}$ for all samples stratigraphically below the Bonarelli Level is −47·1‰, with a range from −45·2 to −51·0‰. While the average $\delta^{34}S_{pyrite}$ across the Bonarelli Level increases to −38·8‰, with a range from −36·8 to −42·6‰. Two analysed samples post-dating the Bonarelli Level yielded values of −34·2‰ and −36·4‰. From these data, it is unclear whether the $\delta^{34}S_{pyrite}$ returns to pre-OAE baseline in strata post-dating the event.

Carbonate sulphur isotopes and iodine/calcium ratios

The $\delta^{34}S_{CAS}$ data were only generated for the carbonate-rich intervals. From the base of the section to the base of the Bonarelli Level, $\delta^{34}S_{CAS}$ is relatively stable with a range from 15·8 to 18·3‰ with a trend towards more positive values as it approaches the Bonarelli Level black shales. This trend of increasing $\delta^{34}S_{CAS}$ continues in the carbonate facies that follows the OAE black shale interval, rising to values near 22‰ at 3·5 m above the top of the Bonarelli Level. The $\Delta^{34}S$, defined as the difference between $\delta^{34}S_{CAS,}$ representing seawater sulphate (Kampschulte & Strauss, 2004), and $\delta^{34}S_{pyrite}$, was calculated for the six samples with both $\delta^{34}S_{CAS}$ and $\delta^{34}S_{pyrite}$ values. From these data, a trend in $\Delta^{34}S$ is suggested, with values rising up-section going into the OAE and falling again higher in the section (Fig. 4).

Overall, the I/Ca results reveal a systematic trend most easily described in three stages: (i) the I/Ca ratios are stable at *ca* 0·6 μmol mol^{-1} for the stratigraphically lowest 5 m; and (ii) decrease to an average of 0·25 μmol mol^{-1} from 5 m to the base of the Bonarelli Level; and then (iii) steadily increase from near 0·25 μmol mol^{-1} to >1 μmol mol^{-1} at higher stratigraphic levels (Fig. 4). No iodine or CAS data are available for the Bonarelli Level because of the absence of carbonate.

DISCUSSION

Local geochemical conditions

The trace-metal record for Furlo has been discussed previously (Turgeon & Brumsack, 2006) and at a nearby section (Scopelliti *et al.*, 2006; Westermann *et al.*, 2014). However, this study provides the first independent geochemical measure of the local redox conditions in a multi-lithology section deposited prior to, during and subsequent to the Oceanic Anoxic Event (OAE) – as an essential interpretive framework for the trace-metal data. For example, the Fe speciation results provide an independent constraint on the local redox environment prior to and during the OAE, but not following due to the presence of carbonate-dominated lithologies. The Fe_{HR}/Fe_T values of black shales throughout the section are elevated relative to typical oxic modern marine sediments (Raiswell & Canfield, 1998; Poulton & Canfield, 2011), suggesting deposition within anoxic bottom waters. The Fe_{py}/Fe_{HR} ratio in the organic-rich layers deposited prior to the OAE must be viewed with caution, because there are only a few results from thin shale interbeds; however, they are all below the euxinic threshold of 0·7 (März *et al.*, 2008), suggesting ferruginous conditions locally (Poulton & Canfield, 2011). Relatively short-term ferruginous conditions have also been documented from Tarfaya in the proto-North Atlantic before and during OAE 2 (Poulton *et al.*, 2015), which is attributed to orbitally forced enhanced continental weathering flux, and similar results are documented for Cretaceous OAE 3 (März *et al.*, 2008). Samples from the Bonarelli Level deposited during the OAE exhibit elevated Fe_{HR}/Fe_T and Fe_{py}/Fe_{HR} consistent with at least local euxinic deposition for these sediments. Therefore, the Fe_{HR}/Fe_T and Fe_{py}/Fe_{HR} data point to the possibility of a shift from pre-OAE anoxic ferruginous to euxinic bottom-water conditions during the OAE for the organic-rich sediments of the Bonarelli Level.

Ferruginous and euxinic conditions, as suggested by Fe speciation, typically enrich Fe relative to Al, but the samples deposited prior to the OAE that otherwise suggest ferruginous conditions fall within the crustal average, while the euxinic OAE samples in the Bonarelli Level are relatively enriched in total Fe. A possible explanation for the lower than expected total Fe content in the black shales deposited prior to the OAE is a lower than typical detrital Fe/Al ratio. On the other hand, the enrichments in the Bonarelli Level suggest either a more active Fe transport and efficient trapping (as in the Fe 'shuttle'; Owens *et al.*, 2012) or a larger hydrothermal contribution during the OAE proper (Jenkyns *et al.*, 2017), with enrichment

facilitated by locally euxinic conditions and associated Fe scavenging as pyrite. Significantly, pyrite framboid diameters in the Bonarelli Level at Furlo average *ca* 7 μm, whereas those in the underlying black shales are larger and less common, with an average diameter of 9·8 μm, further suggesting euxinic conditions once the OAE began (Jenkyns *et al.*, 2007).

Manganese concentrations in the black shales deposited prior to the OAE are below the shale average and decrease further within the Bonarelli Level, a pattern that is attributed here to local syn-sedimentary reduction of Mn oxides under low-oxygen conditions and recycling into the water column (Turgeon & Brumsack, 2006). Trace-metal proxies requiring low-oxygen but not necessarily sulphidic conditions – Cr/Ti, V and Zn (Algeo, 2004; Sahoo *et al.*, 2012; Reinhard *et al.*, 2013; Scott *et al.*, 2013) – show enriched values in sediments deposited prior to the Bonarelli Level. However, all three elements decline to near crustal values within the Bonarelli Level, despite indications from the Fe speciation for more reducing (sulphidic) local conditions that should have continued to enrich these trace metals (Algeo & Maynard, 2004) (see discussion below). Moreover, Mo, a reliable indicator of redox variability, especially euxinic conditions, shows minimal enrichment in sediments deposited prior to the Bonarelli Level and elevated values (≤*ca* 40 ppm) in the Bonarelli Level. These OAE black shale enrichments are on the low end of those typical of modern open-ocean euxinic basins (Scott & Lyons, 2012). The Mo values recorded prior to the OAE suggest that sulphide was accumulating in, but was largely restricted to, the underlying sedimentary pore fluids (Scott & Lyons, 2012). The somewhat muted Mo values characteristic of the Bonarelli Level point to euxinia but with somewhat limited Mo uptake related to global inventory control (see discussion below). It is important to point out that, prior to the deposition of the Bonarelli Level, trace metals suggest only local to regional reduction of oxic conditions, as confirmed by Fe speciation results. However, at the onset of the Bonarelli Level, trace metals began to record the onset of reducing conditions in the global ocean (see discussion below).

The $\delta^{34}S_{CAS}$ record at Furlo is very similar to other high-resolution Italian data sets (Ohkouchi *et al.*, 1999; Owens *et al.*, 2013; Gomes *et al.*, 2016). All of the published $\delta^{34}S_{CAS}$ data from Italy show a *ca* 6 to 7‰ excursion coincident with the carbon-isotope excursion. However, the absolute values for the baseline and associated maximum from the new data set are most similar to those of Ohkouchi *et al.* (1999), who sampled a nearby outcrop of the pelagic Scaglia Bianca. Somewhat different is the record from shallow-water platform carbonates situated much further south at Raia del Pedale, which might have formed from a water mass with a different and perhaps stronger local overprint (Owens *et al.*, 2013). At Furlo, the $\delta^{34}S_{pyrite}$ record is relatively stable prior to the event with a large $\Delta^{34}S$, which suggests pyrite formation in an open system (Sageman *et al.*, 2014) probably near the sediment–water interface but not in the water column, based on the relatively large framboid size (Jenkyns *et al.*, 2007) and minimal Mo enrichment. Through the Bonarelli Level, $\delta^{34}S_{pyrite}$ shifts to more positive values and continues to increase above the black shale. This rise in $\delta^{34}S_{pyrite}$ was more rapid than that of $\delta^{34}S_{CAS}$, which causes the $\Delta^{34}S$ fractionation to decrease slightly from *ca* −62·5 to *ca* −55‰ – similar to the shift seen in the Western Interior Seaway over approximately the same interval (Adams *et al.*, 2010). It is unlikely that this shift was due to local redox changes since the Fe speciation data suggest that local redox conditions became more reducing (i.e. switched from ferruginous to euxinic). If anything, it would be expected that $\Delta^{34}S$ values would be more steady and/or larger during the OAE because the pyrite would be forming in a relatively open-system euxinic water column.

Iodine/calcium ratios reflect concentrations of iodate (IO_3^-) in the water column, because IO_3^- is the only iodine species that is incorporated into precipitating carbonate minerals (Lu *et al.*, 2010). Importantly, local IO_3^- accumulation requires the presence of dissolved oxygen. Quantitative reduction to iodide occurs in oxygen-poor waters with reducing potentials similar to those supporting manganese reduction and denitrification (Wong & Brewer, 1977; Emerson *et al.*, 1979; Rue *et al.*, 1997). On the most basic level, the simple presence of carbonate-bound iodine at Furlo implies that oxygen was present in the shallow waters, which is also confirmed by the presence of pelagic carbonate formed from nannofossils and planktonic foraminifera (Lu *et al.*, 2010, 2016; Zhou *et al.*, 2015).

The I/Ca data set from below the Bonarelli Level shows rather low values throughout the section (<1 μmol mol^{-1}), similar to other recent results for pre-OAE I/Ca ratios at multiple globally dispersed localities (Zhou *et al.*, 2015).

Beyond presence–absence, these I/Ca ratios are extremely low relative to those found in modern well-oxygenated settings, which are typically >2·6 μmol mol^{-1} (Glock *et al.*, 2014; Lu *et al.*, 2016). The I/Ca ratios <2·6 μmol mol^{-1} can be linked to water-column IO_3^- concentrations <250 nM (Lu *et al.*, 2010, 2016; Glock *et al.*, 2014), which are typically observed in marine settings within the oxycline directly overlying anoxic waters (Rue *et al.*, 1997; Lu *et al.*, 2016). By comparison with modern marine IO_3^- concentration profiles and associated sedimentary I/Ca ratios, values of <2·6 μmol mol^{-1} from the Furlo profile here are most parsimoniously linked to carbonate precipitation within the oxycline in a redox-stratified water column (Lu *et al.*, 2016). Similar ranges in I/Ca ratios have been observed at other OAE localities (Lu *et al.*, 2010; Zhou *et al.*, 2015), as well as those crossing the Permian–Triassic boundary (Loope *et al.*, 2013) and from the Palaeoproterozoic (Hardisty *et al.*, 2014), a time of transitional oxygenation with the likelihood of still common anoxic deep waters. Given that the carbonate precipitation might be linked to shallower waters relative to deposition of the studied black shales here, the combined Cr/Ti, V, Mo and Fe_{HR}/Fe_T data from deeper waters and the carbonate I/Ca results from shallow waters strongly suggest a redox-stratified water column – with the possibility of ferruginous bottom waters underlying an oxic surface layer prior to the deposition of the Bonarelli Level. Importantly, the increasing but still low I/Ca ratios relative to modern oxic settings following the OAE suggest a deepening oxycline but with sustained local water-column redox stratification following the event.

Global implications

The Fe geochemistry suggests that this site experienced local euxinic deposition during the OAE; however, trace-metal enrichments are relatively muted for a site experiencing euxinic conditions. An analogous relationship is observed at another OAE 2 locality – including ODP Site 1258, Demerara Rise, eastern equatorial Atlantic (Hetzel *et al.*, 2009; Algeo & Rowe, 2011; Owens *et al.*, 2016) – which suggests a global expansion of reducing conditions during the OAE. Such a hypothesized expansion of reducing conditions depleted the marine inventories of redox-sensitive metals. At this ODP site, molybdenum concentrations do increase at the onset of the OAE, reflecting the beginning of local euxinia, but the values are muted relative to those in modern euxinic settings (Scott & Lyons, 2012). In general, marginal marine sediments lack large trace-metal enrichments during the OAE because there is a global overabundance of sinks (anoxic waters and sediments) in many areas of the ocean compared to the relatively small supply (ocean inventory) of redox-sensitive trace metals. This trend, observed at Furlo as well as other contemporaneous localities, strongly suggests global drawdown of the marine Mo reservoir (reviewed in Owens *et al.*, 2016; Dickson *et al.*, 2017). Previous studies have attributed similar trends to non-euxinic local conditions during the OAE, which would limit the intensity of local Mo scavenging (i.e. Turgeon & Brumsack, 2006; Westermann *et al.*, 2014). However, the addition of Fe speciation data, which indicates persistent local euxinia throughout the OAE interval at Furlo, suggests that the ultimate control on enrichment was ocean-scale expansion of euxinic conditions leading to drawdown of trace elements in seawater on a global scale. The same argument can now be made for other OAE 2 locations.

Additionally, the Mo/TOC ratio drops through the Bonarelli Level to concentrations that are low, even when compared to the non-euxinic deposition prior to the OAE, which further highlights the likelihood of Mo burial under a highly depleted marine reservoir (Algeo & Lyons, 2006; Lyons *et al.*, 2009). The Mo–TOC relationship is well-documented in the modern and ancient ocean for euxinic deposition and manifests itself as strong positive covariation, but the specifics of that relationship vary among different marine basins and intervals of time (Algeo & Lyons, 2006; Scott *et al.*, 2008). It is likely that different mean ratios (slopes of the lines of covariation) track the size of the Mo inventory as related to either local or global factors (Algeo & Lyons, 2006). As such, varying Mo/TOC ratios allow for interpretations that 'see through' local organic matter controls to isolate possible reservoir relationships. Within the Bonarelli Level, the Mo/TOC data average *ca* 3·2 (slightly higher than the 2·8 observed at Site 1258 on Demerara Rise). The Mo/TOC values recorded during the OAE at both Furlo and Demerara Rise are lower than those of the Mo-depleted modern Black Sea (average of *ca* 4·5), while the Mo-replete Cariaco Basin records Mo/TOC values above *ca* 20 (Algeo & Lyons, 2006). In the case of these two modern settings, levels of enrichment are controlled by the strength of the basin's connection

to the open ocean, and thus the renewal time of deep waters relative to the rates of Mo uptake, as well as the timescales and magnitudes of water-column sulphide accumulation. The data from Furlo and many other localities (Owens *et al.*, 2016; Dickson *et al.*, 2017) mirror this inventory relationship where the sediment enrichment in reducing basins outpaces the renewal rate. Thus, the Mo, and likely other redox-sensitive trace metals, drawdown is best explained as an expansion of euxinia during the OAE – compared with conditions before and after the event and in today's ocean.

Trace-metal availability may have played a role in controlling the spatial and temporal patterns of evolution during the Proterozoic when widespread ferruginous and euxinic conditions depleted the seawater concentrations of key elements (Anbar & Knoll, 2002; Scott *et al.*, 2008; Dupont *et al.*, 2010; Planavsky *et al.*, 2010; Reinhard *et al.*, 2013), and similar conditions may have existed for short periods in the Phanerozoic (Gill *et al.*, 2011b). For example, widespread reducing conditions can limit the availability of Mo and V, which are linked to the nitrogen cycle as enzymatic co-factors in nitrogen fixation (Glass *et al.*, 2009; Bellenger *et al.*, 2011; Reinhard *et al.*, 2013). Additionally, Zn is known to be essential for eukaryotic development through protein–DNA interactions (Dupont *et al.*, 2006). Somewhat surprisingly, existing trends suggest that Zn was not limiting in the widely ferruginous and euxinic Proterozoic ocean (Scott *et al.*, 2013). However, concentrations of Zn during the OAE at Furlo and Demerara Rise (Hetzel *et al.*, 2009; Owens *et al.*, 2016) average 91 ppm and 162 ppm, respectively, which is approaching the shale average of *ca* 95 ppm (Turekian & Wedepohl, 1961). In particular, these muted enrichments stand out relative to the average pre-OAE values of 612 ppm observed in the shales. Furthermore, even these higher concentrations are on the low end of what is observed generally during the Precambrian and Phanerozoic in euxinic settings – i.e. values commonly above 500 ppm and extending to values greater than 1000 ppm (Scott *et al.*, 2013). A drawdown of Zn concentrations may have played an important role ecologically during the OAE (Dupont *et al.*, 2006). It is difficult to separate the relative importance of each bio-essential trace element, but collectively limitations are likely to have had important ecological and evolutionary impacts during this time interval.

The sulphur-isotope data for carbonate-associated sulphur (CAS) show a positive excursion just below the Bonarelli Level and the pyrite excursion that starts at the base of the Bonarelli Level, with both continuing towards more positive values into the post-event interval. This excursion, despite the likelihood of regional differences and related local controls, is observed at numerous locations and basins and thus suggests a global perturbation in the sulphur-isotope composition of the ocean. This perturbation is reasonably attributed to a global increase in pyrite burial as the ocean became more reducing, leaving the marine sulphate reservoir isotopically heavy (Ohkouchi *et al.*, 1999; Adams *et al.*, 2010; Owens *et al.*, 2013; Gomes *et al.*, 2016). Specifically, the $\delta^{34}S_{CAS}$ expression of this excursion has now been observed at seven locations worldwide but with varying magnitudes (2 to 7‰), highlighting the combined global and local controls. It is noteworthy that the data of the present study show the global sulphur-isotope trend in both CAS and pyrite isotope data, including pyrite extracted from both shales and carbonate lithologies. Furthermore, the timing and lag following the carbon-isotope excursion are nearly identical at all localities (Ohkouchi *et al.*, 1999; Adams *et al.*, 2010; Owens *et al.*, 2013). However, the positive $\delta^{34}S_{pyrite}$ excursion here of *ca* 12‰ has not been reproduced at other sites (Gautier, 1987; Böttcher *et al.*, 2006; Hetzel *et al.*, 2009; Adams *et al.*, 2010), and the $\Delta^{34}S$ recorded at Furlo prior to the OAE (64·5‰) is the largest known for this event, although it is similar to the values recorded in the Western Interior Seaway (Adams *et al.*, 2010). It is also important to point out that organic sulphur probably plays an important role during this large carbon burial event, but there are very limited data. Finally, it is apparent that $\Delta^{34}S$ decreases post-OAE, but the timing is unclear because there are no CAS data at this site from the carbonate-free Bonarelli Level (Fig. 4).

The I/Ca trend and magnitudes observed at Furlo are consistent with data obtained from previously studied OAE 2 localities, with a switch to low I/Ca ratios beginning below the onset of the positive carbon-isotope excursion (Lu *et al.*, 2010; Zhou *et al.*, 2015). However, unlike the trace-metal records, this response is not easily linked to global iodine inventory shifts, as I/Ca tracks IO_3^- not total dissolved iodine. A lack of a prominent inventory control on I/Ca is supported by OAE 2 trends that vary in timing and magnitude among sites recording intervals

preceding and during the OAE (Zhou *et al.*, 2015). Indeed, organic carbon cycling plays a role in modulating I/Ca ratios, because iodine is a biophilic element whose reservoir size is most strongly linked to organic carbon burial and remineralization (Lu *et al.*, 2010). Consequently, a reservoir shift to lower iodine concentrations might be expected in association with the increase in organic carbon burial that drove the positive carbon-isotope excursion of OAE 2 (Lu *et al.*, 2010). However, the onset of this shift would be anticipated to propagate similarly among localities and to track the change in carbon isotopes if I/Ca ratios were mostly mirroring the total dissolved iodine inventory. As such, the combined I/Ca evidence from Furlo and other localities (Lu *et al.*, 2010; Zhou *et al.*, 2015) instead provide strong evidence for the onset of mildly reducing conditions and a shift towards redox-stratified water columns that decreased local IO_3^- concentrations prior to the OAE. The observed inter-site differences in the timing of I/Ca decreases are consistent with shifts towards low-oxygen, redox-stratified water columns that differed among settings on local and regional scales and may provide new perspectives on the mechanisms behind OAEs (Zhou *et al.*, 2015). Towards that goal, this study is the first to integrate I/Ca ratios from carbonates with other proxy measurements from shales, such as V and Cr/Ti, which are similarly sensitive to subtle variations in dissolved oxygen (Rue *et al.*, 1997). Overall, agreement among the diverse proxies further validates the suggestion of an early onset of low-oxygen conditions prior to the OAE.

CONCLUSIONS

Paired lithofacies and geochemical data from Furlo, Marche–Umbria, Italy, illuminate the local and global redox landscape before and at the onset of Oceanic Anoxic Event 2 (OAE 2). New Fe speciation data delineate local redox conditions during the deposition of the thin black shales below the Bonarelli Level and suggest deposition under ferruginous conditions, with $Fe_{HR}/Fe_T > 0{\cdot}38$ but Fe_{py}/Fe_{HR} well below 0·7. In this pre-OAE interval, redox-sensitive elements that first respond to pronounced oxygen deficiency – Mn, V, Cr/Ti and Zn – are enriched, relative to average shale, with the exception of Mn, which shows a depletion. Furthermore, Mo, a euxinic proxy, shows very limited enrichment in sediments deposited before the Bonarelli Level, consistent with dissolved sulphide being restricted to pore waters in the underlying sediment column. The entire suite of geochemical data from just below the Bonarelli Level points towards local reducing bottom waters that lacked oxygen and sulphide accumulation.

Coincident with the initial onset of deposition at the Bonarelli Level, the Fe proxies suggest bottom-water euxinia, as indicated by parallel enrichments in Fe_{HR}/Fe_T and Fe_{py}/Fe_{HR} and supported by the size distribution of pyrite framboids. Molybdenum values are enriched by up to *ca* 40 ppm, which is similar to euxinic enrichments seen at Demerara Rise in the OAE 2 black shales (Hetzel *et al.*, 2009). These values, however, are relatively subdued compared to modern open-ocean euxinic conditions despite analogously open conditions, suggesting deposition within a depleted dissolved marine Mo reservoir due to global expansion of euxinia (reviewed in Owens *et al.*, 2016; Dickson *et al.*, 2017). Similar relationships have been observed for other intervals in Earth history (Reinhard *et al.*, 2013). Importantly, V, Cr and Zn associated with the euxinic OAE interval are present at close to crustal averages, suggesting analogous drawdown of the marine inventories. Importantly, the expansion of anoxia and euxinia specifically during the OAE probably reduced the global marine metal supplies to levels that might have become biologically limiting. Again, local redox controls are ruled out because of the independent indications of anoxia and euxinia based on Fe proxies.

The carbonate proxies show trends similar to those of previous studies (Ohkouchi *et al.*, 1999; Adams *et al.*, 2010; Lu *et al.*, 2010; Owens *et al.*, 2013; Zhou *et al.*, 2015). Specifically, the $\delta^{34}S_{CAS}$ data show a *ca* 6‰ positive excursion with a slight rise before the Oceanic Anoxic Event that continues post-OAE, suggesting continued euxinic burial of pyrite on a large scale that waned with time (Owens *et al.*, 2013). The relatively low I/Ca ratios recorded prior to the OAE point to an oxic surface ocean in direct exchange with laterally and vertically proximal anoxic water masses, suggesting a shallow pre-OAE chemocline. Following the OAE, the data suggest a deepening of the chemocline related to an expansion of oxygenated waters.

This new multiproxy lithofacies approach applied to carbonates and shales reveals strong consistency prior to the OAE interval and the environmental drivers that spawned alternating

shale and carbonate deposition are not straightforwardly linked to major changes in bottom-water redox conditions. However, no such comparison can be made for the Bonarelli Level due to its lack of carbonate. The stratigraphically higher levels above the Bonarelli Level lack organic-rich shales. Nonetheless, for the first time, the combined shale–carbonate strategy suggests relatively low-oxygen conditions during the deposition of the pre-Bonarelli Level limestones and ferruginous conditions for the interbedded black shales – and thus consistently low O_2 conditions prior to the OAE at this location. Rather than changing redox, the rhythmic deposition was probably tied to other astronomically forced climatic and environmental changes (Galeotti *et al.*, 2009; Lanci *et al.*, 2010). The data set for this study increases current understanding of the spatial extent of reducing conditions and euxinia specifically during OAE 2, with euxinia previously modelled to have affected between 2% and 10% of the sea floor (Owens *et al.*, 2013; Dickson *et al.*, 2016a,b). Consistent with these models, this data set can be added to the growing list of localities that experienced low-oxygen and even ferruginous conditions prior to OAE 2, but it is unlikely that these conditions prevailed globally as trace-metal enrichments remained high (Hetzel *et al.*, 2009; Owens *et al.*, 2016) – perhaps as a first step towards the more extreme conditions of the OAE proper.

ACKNOWLEDGEMENTS

Samples were obtained by JDO, CL and HCJ on a field trip for The Urbino Summer School in Paleoclimatology with an NSF fellowship for JDO and CL. The U.S. National Science Foundation and NASA provided funds for this research (TWL and JDO). ZL was supported by NSF OCE 1232620. We thank Steve Bates for help with sulphur-isotope analyses. The manuscript was improved through reviews by two anonymous reviewers and Stéphane Bodin.

REFERENCES

Adams, D.D., **Hurtgen, M.T.** and **Sageman, B.B.** (2010) Volcanic triggering of a biogeochemical cascade during Oceanic Anoxic Event 2. *Nat. Geosci.*, **3**, 201–204.

Algeo, T.J. (2004) Can marine anoxic events draw down the trace element inventory of seawater? *Geology*, **32**, 1057–1060.

Algeo, T.J. and **Lyons, T.W.** (2006) Mo–total organic carbon covariation in modern anoxic marine environments: implications for analysis of paleoredox and paleohydrographic conditions. *Paleoceanography*, **21**, PA1016 doi:10.1029/2004PA001112.

Algeo, T.J. and **Maynard, J.B.** (2004) Trace-element behavior and redox facies in core shales of Upper Pennsylvanian Kansas-type cyclothems. *Chem. Geol.*, **206**, 289–318.

Algeo, T.J. and **Rowe, H.** (2011) Paleoceanographic applications of trace-metal concentration data. *Chem. Geol.*, **324–325**, 6–18.

Anbar, A.D. and **Knoll, A.H.** (2002) Proterozoic ocean chemistry and evolution: a bioinorganic bridge? *Nature*, **297**, 1137–1142.

Arthur, M.A. and **Premoli-Silva, I.** (1982) Development of widespread organic carbon-rich strata in the Mediterranean Tethys. In: *Nature and Origin of Cretaceous Carbon-rich Facies*. (Eds S.O. Schlanger and M.B. Cita), pp. 7–54. Academic Press, New York.

Arthur, M.A., **Jenkyns, H.C.**, **Brumsack, H.J.** and **Schlanger, S.O.** (1990) Stratigraphy, geochemistry, and paleoceanography of organic carbon-rich Cretaceous sequences. In: *Cretaceous Resources Events and Rhythms* (Eds R.N. Ginsburg and B. Beaudoin), NATO ASI Series C, Kluwer Academic Publishers, **304**, 75–119.

Bambach, R.K. (2006) Phanerozoic biodiversity mass extinctions. *Annu. Rev. Earth Planet. Sci.*, **34**, 127–155.

Batenburg, S.J., **De Vleeschouwer, D.**, **Sprovieri, M.**, **Hilgen, F.J.**, **Gale, A.S.**, **Singer, B.S.**, **Koeberl, C.**, **Coccioni, R.**, **Claeys, P.** and **Montanari, A.** (2016) Orbital control on the timing of oceanic anoxia in the Late Cretaceous. *Clim. Past*, **12**, 1995–2009.

Beaudoin, B., **M'Ban, E.P.**, **Montanari, A.** and **Pinault, M.** (1996) Lithostratigraphie haute resolution (<20 ka) dans le Cénomanien du basin d'Ombrie-Marches. *Comptes Rendus de l'Académie des Sciences, Paris, Série IIa*, **323**, 689–696.

Bellenger, J.P., **Wichard, T.**, **Xu, Y.** and **Kraepiel, A.M.L.** (2011) Essential metals for nitrogen fixation in a free-living N_2-fixing bacterium: chelation, homeostasis and high use efficiency. *Environ. Microbiol.*, **13**, 1395–1411.

van Bentum, E.C., **Hetzel, A.**, **Brumsack, H.-J.**, **Forster, A.**, **Reichart, G.-J.** and **Sinninghe Damsté, J.S.** (2009) Reconstruction of water column anoxia in the equatorial Atlantic during the Cenomania-Turonian oceanic anoxic event using biomarker and trace metal proxies. *Palaeogeogr. Palaeoclimatol. Palaeoecol.*, **280**, 489–498.

Berner, R.A. (2006) GEOCARBSULF: a combined model for Phanerozoic atmospheric O_2 and CO_2. *Geochim. Cosmochim. Acta*, **70**, 5653–5664.

Bernoulli, D. and **Jenkyns, H.C.** (2009) Ancient oceans and continental margins of the Alpine-Mediterranean Tethys: deciphering clues from Mesozoic pelagic sediments and ophiolites. *Sedimentology*, **56**, 149–190.

Blättler, C.L., **Jenkyns, H.C.**, **Reynard, L.M.** and **Henderson, G.M.** (2011) Significant increases in global weathering during Oceanic Anoxic Events 1a and 2 indicated by calcium isotopes. *Earth Planet. Sci. Lett.*, **309**, 77–88.

Blumenberg, M. and **Wiese, F.** (2012) Imbalanced nutrients as triggers for black shale formation in a shallow shelf setting during the OAE 2 (Wunstorf, Germany). *Biogeosciences*, **9**, 4139–4153.

Böttcher, M.E., **Hetzel, A.**, **Brumsack, H.J.** and **Schipper, A.** (2006) Sulfur–iron–carbon geochemistry in sediments of the Demerara Rise. In: *Proceedings of the Ocean Drilling*

Program (Eds D.C. Mosher, J. Erbacher and M.J. Malone), Scientific Results, vol. **207**. Ocean Drilling Program, College Station, TX, pp. 1–23.

Bralower, T.J. (1988) Calcareous nannofossil biostratigraphy and assemblages of the Cenomanian-Turonian boundary interval: implications for the origin and timing of oceanic anoxia. *Paleoceanography*, **3**, 275–316.

Brumsack, H.-J. (2006) The trace metal content of recent organic carbon-rich sediments: implications for Cretaceous black shale formation. *Palaeogeogr. Palaeoclimatol. Palaeoecol.*, **232**, 344–361.

Canfield, D.E., **Raiswell, R.**, **Westrich, J.T.**, **Reaves, C.M.** and **Berner, R.A.** (1986) The use of chromium reduction in the analysis of reduced inorganic sulfur in sediments and shales. *Chem. Geol.*, **54**, 149–155.

Canfield, D.E., **Raiswell, R.** and **Bottrell, S.H.** (1992) The reactivity of sedimentary iron minerals toward sulfide. *Am. J. Sci.*, **292**, 659–683.

Chai, J.Y. and **Muramatsu, Y.** (2007) Determination of bromine and iodine in twenty-three geochemical reference materials by ICP-MS. *Geostand. Geoanal. Res.*, **31**, 143–150.

Clarkson, M.O., **Poulton, S.W.**, **Guilbaud, R.** and **Wood, R.A.** (2014) Assessing the utility of Fe/Al and Fe-speciation to record water column redox conditions in carbonate-rich sediments. *Chem. Geol.*, **382**, 111–122.

Coccioni, R., **Sideri, M.**, **Frontalini, F.** and **Montanari, A.** (2016) The *Rotalipora cushmani* extinction at Gubbio (Italy): Planktonic foraminiferal testimonial of the onset of the Caribbean large igneous province emplacement? In: *The Stratigraphic Record of Gubbio: Integrated Stratigraphy of the Late Cretaceous-Paleogene Umbria-Marche Pelagic Basin* (Eds M. Menichetti, R. Coccioni and A. Montanari), *Geol. Soc. Am, Spec. Paper*, **524**, 79–96.

Dickson, A.J., **Jenkyns, H.C.**, **Porcelli, D.**, **van den Boorn, S.**, **Idiz, E.** and **Owens, J.D.** (2016a) Corrigendum to "Basin-scale controls on the molybdenum-isotope composition of seawater during Oceanic Anoxic Event 2 (Late Cretaceous)". *Geochim. Cosmochim. Acta*, **189**, 404–405.

Dickson, A.J., **Jenkyns, H.C.**, **Porcelli, D.**, **van den Boorn, S.** and **Idiz, E.** (2016b) Basin-scale controls on the molybdenum-isotope composition of seawater during Oceanic Anoxic Event 2 (Late Cretaceous). *Geochim. Cosmochim. Acta*, **178**, 291–306.

Dickson, A.J., **Saker-Clark, M.**, **Jenkyns, H.C.**, **Bottini, C.**, **Erba, E.**, **Russo, F.**, **Gorbanenko, O.**, **Naafs, B.D.A.**, **Pancost, R.D.**, **Robinson, S.A.**, **van den Boorn, S.** and **Idiz, E.** (2017) A Southern Hemisphere record of global trace-metal drawdown and orbital modulation of organic-matter burial across the Cenomanian-Turonian boundary (Ocean Drilling Program Site 1138, Kerguelen Plateau). *Sedimentology*, **64**, 185–202 doi:10.1111/sed.12303, in press.

Du Vivier, A.D.C., **Selby, D.**, **Sageman, B.B.**, **Jarvis, I.**, **Gröcke, D.R.** and **Voigt, S.** (2014) Marine $^{187}Os/^{188}Os$ isotope stratigraphy reveals the interaction of volcanism and ocean circulation during Oceanic Anoxic Event 2. *Earth Planet. Sci. Lett.*, **389**, 23–33.

Du Vivier, A.D.C., **Selby, D.**, **Condon, D.J.**, **Takashima, R.** and **Nishi, H.** (2015) Pacific $^{187}Os/^{188}Os$ isotope chemistry and U-Pb geochronology: synchroneity of global Os isotope change across OAE 2. *Earth Planet. Sci. Lett.*, **428**, 204–216.

Dupont, C.L., **Yang, S.**, **Palenik, B.** and **Bourne, P.E.** (2006) Modern proteomes contain putative imprints of ancient shifts in trace metal geochemistry. *Proc. Natl Acad. Sci.*, **103**, 17822–17827.

Dupont, C.L., **Butcher, A.**, **Valas, R.E.**, **Bourne, P.E.** and **Caetano-Anollés, G.** (2010) History of biological metal utilization inferred through phylogenomic analysis of protein structures. *Proc. Natl Acad. Sci.*, **107**, 10567–10572.

Elder, W.P. (1991) Molluscan paleoecology and sedimentation patterns of the Cenomanian-Turonian extinction interval on the southern Colorado Plateau region. In: *Stratigraphy, Depositional Environments, and Sedimentary Tectonics of the Western Margin, Cretaceous Western Interior Seaway*. (Eds J.D. Nations and J.G. Eaton), *Geol. Soc. Am. Spec. Pap.*, **260**, 113–138.

Elder, W. and **Kirkland, J.** (1985) Stratigraphy and depositional environments of the Bridge Creek Limestone Member of the Greenhorn Limestone at Rock Canyon Anticline near Pueblo, Colorado. In: *Fine-grained deposits and biofacies of the CretaceousWestern Interior Seaway: evidence of cyclic depositional processes*. (Eds L. Pratt, E.G. Kauffman and F.B. Zelt), SEPM Annual Mid-year Meeting, Field Trip No. 9, pp. 122–134.

Eldrett, J.S., **Ma, C.**, **Bergman, S.C.**, **Lutz, B.**, **Gregory, F.J.**, **Dodsworth, P.**, **Phipps, M.**, **Hardas, P.**, **Minisini, D.**, **Ozkan, A.**, **Ramezani, J.**, **Bowring, S.A.**, **Kamo, S.L.**, **Ferguson, K.**, **Macaulay, C.** and **Kelly, A.E.** (2015) An astronomically calibrated stratigraphy of the Cenomanian, Turonian and earliest Coniacian from the Cretaceous Western Interior Seaway, USA: implications for global chronostratigraphy. *Cretac. Res.*, **56**, 316–344.

Emerson, S., **Cranston, R.E.** and **Liss, P.S.** (1979) Redox species in a reducing fjord: equilibrium and kinetic considerations. *Deep Sea Res. A*, **26**, 859–878.

Erba, E. (2004) Calcareous nannofossils and Mesozoic oceanic anoxic events. *Mar. Micropaleontol.*, **52**, 85–106.

Erbacher, J. and **Thurow, J.** (1997) Influence of oceanic anoxic events on the evolution of mid-Cretaceous radiolaria in the North Atlantic and western Tethys. *Mar. Micropaleontol.*, **30**, 139–158.

Erbacher, J., **Thurow, J.** and **Littke, R.** (1996) Evolution patterns of radiolaria and organic matter variations: a new approach to identify sea-level changes in mid-Cretaceous pelagic environments. *Geology*, **24**, 499–502.

Farrimond, P., **Eglinton, G.**, **Brassell, S.C.** and **Jenkyns, H.C.** (1990) The Cenomanian/Turonian anoxic event in Europe: an organic geochemical study. *Mar. Pet. Geol.*, **7**, 75–89.

Friedrich, O., **Norris, R.D.** and **Erbacher, J.** (2012) Evolution of middle to Late Cretaceous oceans—A 55 m.y. record of Earth's temperature and carbon cycle. *Geology*, **40**, 107–110.

Galeotti, S., **Rusciadelli, G.**, **Sprovieri, M.**, **Lanci, L.**, **Gaudio, A.** and **Pekar, S.** (2009) Sea-level control on facies architecture in the Cenomanian-Coniacian Apulian margin (Western Tethys): a record of glacio-eustatic fluctuations during the Cretaceous greenhouse? *Palaeogeogr. Palaeoclimatol. Palaeoecol.*, **276**, 196–205.

Gambacorta, G., **Jenkyns, H.C.**, **Russo, F.**, **Tsikos, H.**, **Wilson, P.A.**, **Faucher, G.** and **Erba, E.** (2015) Carbon- and oxygen-isotope records of mid-Cretaceous Tethyan pelagic sequences from the Umbria–Marche and Belluno Basins (Italy). *Newsl. Stratigr.*, **48**, 299–323.

Gautier, D.L. (1987) Isotopic composition of pyrite: relationship to organic matter type and iron availability in some North American Cretaceous shales. *Chem. Geol.*, **65**, 293–303.

Gellatly, A.M. and **Lyons, T.W.** (2005) Trace sulfate in mid-Proterozoic carbonates and the sulfur isotope record of

biospheric evolution. *Geochim. Cosmochim. Acta*, **69**, 3813–3829.

Gill, B.C., **Lyons, T.W.** and **Jenkyns, H.C.** (2011a) A global perturbation to the sulfur cycle during the Toarcian Oceanic Anoxic Event. *Earth Planet. Sci. Lett.*, **312**, 484–496.

Gill, B.C., **Lyons, T.W.**, **Young, S.A.**, **Kump, L.R.**, **Knoll, A.H.** and **Saltzman, M.R.** (2011b) Geochemical evidence for widespread euxinia in the Later Cambrian ocean. *Nature*, **469**, 80–83.

Glass, J.B., **Wolfe-Simon, F.** and **Anbar, A.D.** (2009) Coevolution of metal availability and nitrogen assimilation in cyanobacteria and algae. *Geobiology*, **7**, 100–123.

Glock, N., **Liebetrau, V.** and **Eisenhauer, A.** (2014) I/Ca ratios in benthic foraminifera from the Peruvian oxygen minimum zone: analytical methodology and evaluation as a proxy for redox conditions. *Biogeosciences*, **11**, 7077–7095.

Goldberg, T., **Poulton, S.W.**, **Wagner, T.**, **Kolonic, S.F.** and **Rehkämper, M.** (2016) Molybdenum drawdown during Cretaceous Oceanic Anoxic Event 2. *Earth Planet. Sci. Lett.*, **440**, 81–91.

Gomes, M.L., **Hurtgen, M.T.** and **Sageman, B.B.** (2016) Biogeochemical sulfur cycling during Cretaceous oceanic anoxic events: a comparison of OAE1a and OAE2. *Paleoceanography*, **31**, 233–251.

Haq, B.U., **Hardenbol, J.A.N.** and **Vail, P.R.** (1987) Chronology of fluctuating sea levels since the Triassic. *Science*, **235**, 1156–1167.

Hardisty, D.S., **Lu, Z.**, **Planavsky, N.J.**, **Bekker, A.**, **Philippot, P.**, **Zhou, X.** and **Lyons, T.W.** (2014) An iodine record of Paleoproterozoic surface ocean oxygenation. *Geology*, **42**, 619–622.

Hasegawa, T. (1997) Cenomanian-Turonian carbon isotope events recorded in terrestrial organic matter from northern Japan. *Palaeogeogr. Palaeoclimatol. Palaeoecol.*, **130**, 251–273.

Hetzel, A., **Böttcher, M.E.**, **Wortmann, U.G.** and **Brumsack, H.-J.** (2009) Paleo-redox conditions during OAE 2 reflected in Demerara Rise sediment geochemistry (ODP Leg 207). *Palaeogeogr. Palaeoclimatol. Palaeoecol.*, **273**, 302–328.

Hetzel, A., **März, C.**, **Vogt, C.** and **Brumsack, H.-J.** (2011) Geochemical environment of Cenomanian – Turonian black shale deposition at Wunstorf (northern Germany). *Cretac. Res.*, **32**, 480–494.

Jarvis, I.A.N., **Murphy, A.M.** and **Gale, A.S.** (2001) Geochemistry of pelagic and hemipelagic carbonates: criteria for identifying systems tracts and sea-level change. *J. Geol. Soc.*, **158**, 685–696.

Jenkyns, H.C. (2010) Geochemistry of oceanic anoxic events. *Geochem. Geophys. Geosyst.*, **11**, Q03004.

Jenkyns, H.C., **Matthews, A.**, **Tsikos, H.** and **Erel, Y.** (2007) Nitrate reduction, sulfate reduction, and sedimentary iron isotope evolution during the Cenomanian-Turonian oceanic anoxic event. *Paleoceanography*, **22**, PA3208 doi:10.1029/2006pa001355.

Jenkyns, H.C., **Dickson, A.J.**, **Ruhl, M.** and **Van Den Boorn, S.H.J.M.** (2017) Basalt–seawater interaction, the Plenus Cold Event, enhanced weathering and geochemical change: deconstructing Oceanic Anoxic Event 2 (Cenomanian–Turonian, Late Cretaceous). *Sedimentology*, **64**, 16–43 doi:10.1111/sed.12305, in press.

Jones, C.E. and **Jenkyns, H.C.** (2001) Seawater strontium isotopes, oceanic anoxic events, and seafloor hydrothermal activity in the Jurassic and Cretaceous. *Am. J. Sci.*, **301**, 112–149.

Kaiho, K. and **Hasegawa, T.** (1994) End-Cenomanian benthic foraminiferal extinctions and oceanic dysoxic events in the northwestern Pacific Ocean. *Palaeogeogr. Palaeoclimatol. Palaeoecol.*, **111**, 29–43.

Kampschulte, A. and **Strauss, H.** (2004) The sulfur isotopic evolution of Phanerozoic seawater based on the analysis of structurally substituted sulfate in carbonates. *Chem. Geol.*, **204**, 255–286.

Kraal, P., **Slomp, C.P.**, **Forster, A.** and **Kuypers, M.M.M.** (2010) Phosphorus cycling from the margin to abyssal depths in the proto-Atlantic during oceanic anoxic event 2. *Palaeogeogr. Palaeoclimatol. Palaeoecol.*, **295**, 42–54.

Kuhnt, W., **Luderer, F.**, **Nederbragt, S.**, **Thurow, J.** and **Wagner, T.** (2005) Orbital-scale record of the late Cenomanian-Turonian oceanic anoxic event (OAE-2) in the Tarfaya Basin (Morocco). *Int. J. Earth Sci.*, **94**, 147–159.

Kuroda, J. and **Ohkouchi, N.** (2006) Implication of spatiotemporal distribution of black shales deposited during the Cretaceous Oceanic Anoxic Event-2. *Paleontol. Res.*, **10**, 345–358.

Kuroda, J., **Ogawa, N.O.**, **Tanimizu, M.**, **Coffin, M.F.**, **Tokuyama, H.**, **Kitazato, H.** and **Ohkouchi, N.** (2007) Contemporaneous massive subaerial volcanism and late cretaceous Oceanic Anoxic Event 2. *Earth Planet. Sci. Lett.*, **256**, 211–223.

Kuypers, M.M.M., **Pancost, R.D.**, **Nijenhuis, I.A.** and **Sinninghe Damsté, J.S.** (2002) Enhanced productivity led to increased organic carbon burial in the euxinic North Atlantic basin during the late Cenomanian oceanic anoxic event. *Paleoceanography*, **17**, 1051.

Lanci, L., **Muttoni, G.** and **Erba, E.** (2010) Astronomical tuning of the Cenomanian Scaglia Bianca Formation at Furlo, Italy. *Earth Planet. Sci. Lett.*, **292**, 231–237.

Leckie, R.M. (1985) Foraninifera of the Cenomanian-Turonian Boundary Interval, Greenhorn Formation, Rock Canyon Anticline, Pueblo, Colorado, In: Fine-grained deposits and biofacies of the CretaceousWestern Interior Seaway: evidence of cyclic depositional processes. (Eds L. Pratt, E.G. Kauffman and F.B. Zelt), SEPM Annual Mid-year Meeting, Field Trip No. 4, 5–19.

Leckie, R.M., **Bralower, T.J.** and **Cashman, R.** (2002) Oceanic anoxic events and plankton evolution: biotic response to tectonic forcing during the mid-Cretaceous. *Paleoceanography*, **17**, PA000623 doi:10.1029/2001PA000623.

Loope, G.R., **Kump, L.R.** and **Arthur, M.A.** (2013) Shallow water redox conditions from the Permian-Triassic boundary microbialite: the rare earth element and iodine geochemistry of carbonates from Turkey and South China. *Chem. Geol.*, **351**, 195–208.

Lu, Z., **Jenkyns, H.C.** and **Rickaby, R.E.M.** (2010) Iodine to calcium ratios in marine carbonate as a paleo-redox proxy during oceanic anoxic events. *Geology*, **38**, 1107–1110.

Lu, Z., **Hoogakker, B.A.A.**, **Hillenbrand, C.-D.**, **Zhou, X.**, **Thomas, E.**, **Gutchess, K.M.**, **Lu, W.**, **Jones, L.** and **Rickaby, R.E.M.** (2016) Oxygen depletion recorded in upper waters of the glacial Southern Ocean. *Nat. Commun.*, **7**, 11146. doi:10.1038/ncomms11146.

Lyons, T.W. and **Severmann, S.** (2006) A critical look at iron paleoredox proxies: new insights from modern euxinic marine basins. *Geochim. Cosmochim. Acta*, **70**, 5698–5722.

Lyons, T.W., **Anbar, A.D.**, **Severmann, S.**, **Scott, C.** and **Gill, B.C.** (2009) Tracking euxinia in the ancient ocean: a multiproxy perspective and proterozoic case study. *Annu. Rev. Earth Planet. Sci.*, **37**, 507–534.

MacLeod, K.G., **Martin, E.E.** and **Blair, S.W.** (2008) Nd isotopic excursion across Cretaceous ocean anoxic event 2 (Cenomanian-Turonian) in the tropical North Atlantic. *Geology*, **36**, 811–814.

Martin, E.E., **MacLeod, K.G.**, **Jiménez Berrocoso, A.** and **Bourbon, E.** (2012) Water mass circulation on Demerara Rise during the Late Cretaceous based on Nd isotopes. *Earth Planet. Sci. Lett.*, **327–328**, 111–120.

März, C., **Poulton, S.W.**, **Beckmann, B.**, **Küster, K.**, **Wagner, T.** and **Kasten, S.** (2008) Redox sensitivity of P cycling during marine black shale formation: dynamics of sulfidic and anoxic, non-sulfidic bottom waters. *Geochim. Cosmochim. Acta*, **72**, 3703–3717.

Mitchell, R.N., **Bice, D.M.**, **Montanari, A.**, **Cleaveland, L.C.**, **Christianson, K.T.**, **Coccioni, R.** and **Hinnov, L.A.** (2008) Oceanic anoxic cycles? Orbital prelude to the Bonarelli Level (OAE 2). *Earth Planet. Sci. Lett.*, **267**, 1–16.

Monteiro, F.M., **Pancost, R.D.**, **Ridgwell, A.** and **Donnadieu, Y.** (2012) Nutrients as the dominant control on the spread of anoxia and euxinia across the Cenomanian-Turonian oceanic anoxic event (OAE2): model-data comparison. *Paleoceanography*, **27**, PA4209 doi:10.1029/2012pa002351.

Mort, H., **Jacquat, O.**, **Adatte, T.**, **Steinmann, P.**, **Föllmi, K.**, **Matera, V.**, **Berner, Z.** and **Stüben, D.** (2007) The Cenomanian/Turonian anoxic event at the Bonarelli Level in Italy and Spain: enhanced productivity and/or better preservation? *Cretac. Res.*, **28**, 597–612.

Mort, H.P., **Adatte, T.**, **Keller, G.**, **Bartels, D.**, **Föllmi, K.B.**, **Steinmann, P.**, **Berner, Z.** and **Chellai, E.H.** (2008) Organic carbon deposition and phosphorus accumulation during Oceanic Anoxic Event 2 in Tarfaya, Morocco. *Cretac. Res.*, **29**, 1008–1023.

Musavu-Moussavou, B., **Danelian, T.**, **Baudin, F.**, **Coccioni, R.** and **Fröhlich, F.** (2007) The Radiolarian biotic response during OAE2. A high-resolution study across the Bonarelli level at Bottaccione (Gubbio, Italy). *Rev. Micropaléontol.*, **50**, 253–287.

Nederbragt, A.J. and **Fiorentino, A.** (1999) Stratigraphy and palaeoceanography of the Cenomanian-Turonian Boundary Event in Oued Mellegue, north-western Tunisia. *Cretac. Res.*, **20**, 47–62.

Ohkouchi, N., **Kawamura, K.**, **Kajiwara, Y.**, **Wada, E.**, **Okada, M.**, **Kanamatsu, T.** and **Taira, A.** (1999) Sulfur isotope records around Livello Bonarelli (northern Apennines, Italy) black shale at the Cenomanian-Turonian boundary. *Geology*, **27**, 535–538.

Owens, J.D., **Lyons, T.W.**, **Li, X.**, **Macleod, K.G.**, **Gordon, G.**, **Kuypers, M.M.M.**, **Anbar, A.**, **Kuhnt, W.** and **Severmann, S.** (2012) Iron isotope and trace metal records of iron cycling in the proto-North Atlantic during the Cenomanian-Turonian oceanic anoxic event (OAE-2). *Paleoceanography*, **27**, PA3223 doi:10.1029/2012pa002328.

Owens, J.D., **Gill, B.C.**, **Jenkyns, H.C.**, **Bates, S.M.**, **Severmann, S.**, **Kuypers, M.M.M.**, **Woodfine, R.G.** and **Lyons, T.W.** (2013) Sulfur isotopes track the global extent and dynamics of euxinia during Cretaceous Oceanic Anoxic Event 2. *Proc. Natl Acad. Sci.*, **110**, 18407–18412.

Owens, J.D., **Reinhard, C.T.**, **Rohrssen, M.**, **Love, G.D.** and **Lyons, T.W.** (2016) Empirical links between trace metal cycling and marine microbial ecology during a large perturbation to Earth's carbon cycle. *Earth Planet. Sci. Lett.*, **449**, 407–417.

Pancost, R.D., **Crawford, N.**, **Magness, S.**, **Turner, A.**, **Jenkyns, H.C.** and **Maxwell, J.R.** (2004) Further evidence for the development of photic-zone euxinic conditions during Mesozoic oceanic anoxic events. *J. Geol. Soc.*, **161**, 353–364.

Parente, M., **Frijia, G.**, **Di Lucia, M.**, **Jenkyns, H.C.**, **Woodfine, R.G.** and **Baroncini, F.** (2008) Stepwise extinction of larger foraminifers at the Cenomanian-Turonian boundary: a shallow-water perspective on nutrient fluctuations during Oceanic Anoxic Event 2 (Bonarelli Event). *Geology*, **36**, 715–718.

Pearce, M.A., **Jarvis, I.** and **Tocher, B.A.** (2009) The Cenomanian-Turonian boundary event, OAE2 and palaeoenvironmental change in epicontinental seas: new insights from the dinocyst and geochemical records. *Palaeogeogr. Palaeoclimatol. Palaeoecol.*, **280**, 207–234.

Planavsky, N.J., **Rouxel, O.J.**, **Bekker, A.**, **Lalonde, S.V.**, **Konhauser, K.O.**, **Reinhard, C.T.** and **Lyons, T.W.** (2010) The evolution of the marine phosphate reservoir. *Nature*, **467**, 1088–1090.

Pogge von Strandmann, P.A.E., **Jenkyns, H.C.** and **Woodfine, R.G.** (2013) Lithium isotope evidence for enhanced weathering during Oceanic Anoxic Event 2. *Nat. Geosci.*, **6**, 668–672.

Poulton, S.W. and **Canfield, D.E.** (2005) Development of a sequential extraction procedure for iron: implications for iron partitioning in continentally derived particulates. *Chem. Geol.*, **214**, 209–221.

Poulton, S.W. and **Canfield, D.E.** (2011) Ferruginous Conditions: a Dominant Feature of the Ocean through Earth's History. *Elements*, **7**, 107–112.

Poulton, S.W. and **Raiswell, R.** (2005) Chemical and physical characteristics of iron oxides in riverine and glacial meltwater sediments. *Chem. Geol.*, **218**, 203–221.

Poulton, S.W., **Henkel, S.**, **März, C.**, **Urquhart, H.**, **Flögel, S.**, **Kasten, S.**, **Sinninghe Damsté, J.S.** and **Wagner, T.** (2015) A continental-weathering control on orbitally driven redox-nutrient cycling during Cretaceous Oceanic Anoxic Event 2. *Geology*, **43**, 963–966.

Premoli Silva, I. and **Sliter, W.V.** (1999) Cretaceous paleoceanography: evidence from planktonic foraminiferal evolution. In: *Evolution of the Cretaceous Ocean-Climate System* (Eds E. Barrera and C. Johnson), *Geol. Soc. Am. Spec. Pap.*, **332**, 301–328.

Raiswell, R. and **Canfield, D.E.** (1998) Sources of iron for pyrite formation in marine sediments. *Am. J. Sci.*, **298**, 219–245.

Raiswell, R., **Newton, R.**, **Bottrell, S.H.**, **Coburn, P.M.**, **Briggs, D.E.G.**, **Bond, D.P.G.** and **Poulton, S.W.** (2008) Turbidite depositional influences on the diagenesis of Beecher's Trilobite Bed and the Hunsruck Slate; sites of soft tissue pyritization. *Am. J. Sci.*, **308**, 105–129.

Reinhard, C.T., **Planavsky, N.J.**, **Robbins, L.J.**, **Partin, C.A.**, **Gill, B.C.**, **Lalonde, S.V.**, **Bekker, A.**, **Konhauser, K.O.** and **Lyons, T.W.** (2013) Proterozoic ocean redox and biogeochemical stasis. *Proc. Natl Acad. Sci.*, **110**, 5357–5362.

Rue, E.L., **Smith, G.J.**, **Cutter, G.A.** and **Bruland, K.W.** (1997) The response of trace element redox couples to suboxic conditions in the water column. *Deep Sea Res. Part I*, **44**, 113–134.

Sageman, B.B., **Meyers, S.R.** and **Arthur, M.A.** (2006) Orbital time scale and new C-isotope record for Cenomanian-Turonian boundary stratotype. *Geology*, **34**, 125–128.

Sageman, B.B., **Lyons, T.W.** and **Joo, Y.J.** (2014) 9.6 - Geochemistry of fine-grained, organic carbon-rich facies. In: *Treatise on Geochemistry*, 2nd edn (Ed. K.K. Turekian), pp. 141–179. Elsevier, Oxford.

Sahoo, S.K., **Planavsky, N.J.**, **Kendall, B.**, **Wang, X.**, **Shi, X.**, **Scott, C.**, **Anbar, A.D.**, **Lyons, T.W.** and **Jiang, G.** (2012) Ocean oxygenation in the wake of the Marinoan glaciation. *Nature*, **489**, 546–549.

Schlanger, S.O. and **Jenkyns, H.C.** (1976) Cretaceous oceanic anoxic events: causes and consequences. *Geol. Mijnbouw*, **55**, 179–184.

Schlanger, S.O., **Arthur, M.A.**, **Jenkyns, H.C.** and **Scholle, P.A.** (1987) The Cenomanian-Turonian Oceanic Anoxic Event, I. Stratigraphy and distribution of organic carbon-rich beds and the marine $\delta^{13}C$ excursion. In: *Marine Petroleum Source Rocks* (Eds J. Brooks and A.J. Fleet), Geological Society, Special Publications, London, **26**, 371–399.

Scholle, P.A. and **Arthur, M.A.** (1980) Carbon isotope fluctuations in Cretaceous pelagic limestones; potential stratigraphic and petroleum exploration tool. *AAPG Bull.*, **64**, 67–87.

Scopelliti, G., **Bellanca, A.**, **Neri, R.**, **Baudin, F.** and **Coccioni, R.** (2006) Comparative high-resolution chemostratigraphy of the Bonarelli Level from the reference Bottaccione section (Umbria–Marche Apennines) and from an equivalent section in NW Sicily: consistent and contrasting responses to the OAE2. *Chem. Geol.*, **228**, 266–285.

Scotese, C.R. (2008) The PALEOMAP Project PaleoAtlas for ArcGIS, Volume **2**. *Cretaceous Paleogeographic and Plate Rectonic Reconstructions, PALEOMAP Project*.

Scott, C. and **Lyons, T.W.** (2012) Contrasting molybdenum cycling and isotopic properties in euxinic versus non-euxinic sediments and sedimentary rocks: refining the paleoproxies. *Chem. Geol.*, **324–325**, 19–27.

Scott, C., **Lyons, T.W.**, **Bekker, A.**, **Shen, Y.**, **Poulton, S.W.**, **Chu, X.** and **Anbar, A.D.** (2008) Tracing the stepwise oxygenation of the Proterozoic ocean. *Nature*, **452**, 456–459.

Scott, C., **Planavsky, N.J.**, **Dupont, C.L.**, **Kendall, B.**, **Gill, B.C.**, **Robbins, L.J.**, **Husband, K.F.**, **Arnold, G.L.**, **Wing, B.A.**, **Poulton, S.W.**, **Bekker, A.**, **Anbar, A.D.**, **Konhauser, K.O.** and **Lyons, T.W.** (2013) Bioavailability of zinc in marine systems through time. *Nat. Geosci.*, **6**, 125–128.

Sinninghe Damsté, J.S. and **Köster, J.** (1998) A euxinic southern North Atlantic Ocean during the Cenomanian/Turonian oceanic anoxic event. *Earth Planet. Sci. Lett.*, **158**, 165–173.

Snow, L.J., **Duncan, R.A.** and **Bralower, T.J.** (2005) Trace element abundances in the Rock Canyon Anticline, Pueblo, Colorado, marine sedimentary section and their relationship to Caribbean plateau construction and oxygen anoxic event 2. *Paleoceanography*, **20**, PA3005 doi:10.1029/2004PA001093.

Takashima, R., **Nishi, H.**, **Huber, B.T.** and **Leckie, M.** (2006) Greenhouse world and the Mesozoic Ocean. *Oceanography*, **19**, 82–92.

Tsikos, H., **Jenkyns, H.C.**, **Walsworth-Bell, B.**, **Petrizzo, M.R.**, **Forster, A.**, **Kolonic, S.**, **Erba, E.**, **Premoli Silva, I.**, **Baas, M.**, **Wagner, T.** and **Sinninghe Damsté, J.S.** (2004) Carbon-isotope stratigraphy recorded by the Cenomanian-Turonian Oceanic Anoxic Event: correlation and implications based on three key localities. *J. Geol. Soc.*, **161**, 711–719.

Turekian, K.K. and **Wedepohl, K.H.** (1961) Distribution of the elements in some major units of the earth's crust. *Geol. Soc. Am. Bull.*, **72**, 175–192.

Turgeon, S. and **Brumsack, H.-J.** (2006) Anoxic vs dysoxic events reflected in sediment geochemistry during the Cenomanian-Turonian Boundary Event (Cretaceous) in the Umbria-Marche Basin of central Italy. *Chem. Geol.*, **234**, 321–339.

Van Cappellen, P. and **Ingall, E.D.** (1994) Benthic phosphorus regeneration, net primary production, and ocean anoxia: a model of the coupled marine biogeochemical cycles of carbon and phosphorus. *Paleoceanography*, **9**, 677–692.

Voigt, S., **Erbacher, J.**, **Mutterlose, J.**, **Weiss, W.**, **Westerhold, T.**, **Wiese, F.**, **Wilmsen, M.** and **Wonik, T.** (2008) The Cenomanian – Turonian of the Wunstorf section – (North Germany): global stratigraphic reference section and new orbital time scale for Oceanic Anoxic Event 2. *Newsl. Stratigr.*, **43**, 65–89.

Westermann, S., **Vance, D.**, **Cameron, V.**, **Archer, C.** and **Robinson, S.A.** (2014) Heterogeneous oxygenation states in the Atlantic and Tethys oceans during Oceanic Anoxic Event 2. *Earth Planet. Sci. Lett.*, **404**, 178–189.

Wong, G.T.F. and **Brewer, P.G.** (1977) The marine chemistry of iodine in anoxic basins. *Geochim. Cosmochim. Acta*, **41**, 151–159.

Zerkle, A.L., **House, C.H.**, **Cox, R.P.** and **Canfield, D.E.** (2006) Metal limitation of cyanobacterial N_2 fixation and implications for the Precambrian nitrogen cycle. *Geobiology*, **4**, 285–297.

Zheng, X.-Y., **Jenkyns, H.C.**, **Gale, A.S.**, **Ward, D.J.** and **Henderson, G.M.** (2013) Changing ocean circulation and hydrothermal inputs during Ocean Anoxic Event 2 (Cenomanian-Turonian): evidence from Nd-isotopes in the European shelf sea. *Earth Planet. Sci. Lett.*, **375**, 338–348.

Zhou, X., **Jenkyns, H.C.**, **Owens, J.D.**, **Junium, C.K.**, **Zheng, X.-Y.**, **Sageman, B.B.**, **Hardisty, D.S.**, **Lyons, T.W.**, **Ridgwell, A.** and **Lu, Z.** (2015) Upper ocean oxygenation dynamics from I/Ca ratios during the Cenomanian-Turonian OAE 2. *Paleoceanography*, **30**, 510–526.

Manuscript received 16 August 2016; revision accepted 23 November 2016

Supporting Information

Additional Supporting Information may be found in the online version of this article:

Table S1. Geochemical data for the section.